RSC Advances

ROYAL SOCIETY OF CHEMISTRY

www.rsc.org/advances

Alginate surfactant derivatives as ecofriendly corrosion inhibitor for carbon steel in acidic environment

Salah M. Tawfik*

Egyptian Petroleum Research Institute, Nasr City, Cairo, Egypt.
* Corresponding author: salahtwfk85@yahoo.com, Tel. 002-01273615278.

Abstract

The biopolymer alginate surfactant derivatives were synthesized and their influences as a novel corrosion inhibitor on carbon steel in 1 M HCl were studied using gravimetric, electrochemical, EDX and SEM techniques. The compounds obtained were characterized using FTIR, ^{1}HNMR and UV-Vis spectroscopy studies. The inhibition efficiency increased with the increase in concentration and reached a maximum of 96.27% for AS-Cu at $5x10^{-3}$ M concentration. Potentiodynamic polarization results reveal that alginate derivatives could be classified as mixed-type corrosion inhibitors with predominant control of the cathodic reaction. The extent of inhibition exhibits a positive trend with increase in temperature. Langmuir isotherm provides the best description on the adsorption nature of the inhibitor. The results of EIS indicate that the both charge transfer resistance and inhibition efficiency tend to increase by increasing the inhibitor concentration. Thermodynamic parameter and activation parameters were calculated to investigate mechanism of inhibition. Also, the relationship between chemical structure and inhibition efficiency of the inhibitor was discussed.

***Keywords*:**

Biopolymer; carbon steel; corrosion inhibition; electrochemical; HCl; thermodynamic

1. Introduction

Carbon steel is a common constructional material for many industrial units because of its low cost and excellent mechanical properties. However, it suffers severe attack in service particularly in oil and gas production systems. Use of commercial hydrochloric and sulphuric acids leads to destructive effects on the metal surface during industrial-cleaning processes such as: acid pickling, acid descaling, oil-well acid in oil recovery, and in petrochemical processes. In oil fields, hydrochloric acid solution was recommended as the cheapest way to dissolve calcium carbonate, $CaCO_3$, scale inside the pipelines under most conditions [1,2]. Organic inhibitors get adsorbed easily on the metal surface by donating the lone pair of electrons on

nitrogen, oxygen and sulphur to the vacant orbitals on the metal atoms. Electrons and long side chain in the inhibitor molecule also enhance adsorption on the metal surface [3]. Polymers are the more preferred choice for inhibition, as they provide effective blanketing on the surface of the metal with high chelating ability and large molecular size [4]. Over the past few years, there has been a considerable intolerance towards the usage of molecules, inorganic salts and synthetic polymer inhibitors owing to their toxic nature. Obviously, there is a paradigm to switch over to eco-friendly inhibitors. Awesome number of green inhibitors like plant extracts, vegetable oils, fruit juices, waste materials, etc. have been identified so far [5–13]. Among various green inhibitors, biopolymers are more preferred due to their excellent inhibiting property with multiple adsorption sites as lignin [14], poly caffeic acid [15], polyaspartic acid [16], hydroxyl propyl cellulose [17], and carboxy methyl cellulose [18]. Plant extracts, drugs, amino acids, medicinal products, natural polymers have been advocated by various researchers [19-27]. Interest in natural polymers is principally due to its biodegradability and eco-friendliness in addition to the inherent stability and multiple adsorption centers. A number of naturally occurring polymers have been investigated and have been reported to show promising results as metal corrosion inhibitors in different corrosive environments. For instance the corrosion inhibiting effect of chitosan has been reported for mild steel and copper in acid medium [28-31]. Glucose, gellan gum, and hydroxylpropyl cellulose have been assessed as green inhibitors for cast iron in acidic environment by means of chemical and electrochemical techniques [32]. Gum Arabic has also been reported to be a promising corrosion inhibitor for aluminium and steel in different corrosive environments [33]. Modified cassava starch has also been evaluated as corrosion inhibitors of carbon steel under alkaline conditions in 200 mg L^{-1} NaCl solutions [34].

Alginate is a linear polysaccharide present in the cell walls of the fronds of various seaweeds, including the giant brown kelp (*Macrocystis pyrifera*), horsetail kelp (*Laminaria digitalis*), and sugar kelp (*L. saccharina*). It consists of 1,4-β-D-mannuronic and 1,4-L-guluronic acid residues. It is regarded as biocompatible, non-toxic, non immunogenic and biodegradable which make it widely used for industrial applications. Recently, alginate has been chemically modified to increase its hydrophobicity. Alginate has a number of free hydroxyl and carboxyl groups distributed along the backbone, therefore it is an ideal candidate for chemical functionalization [35]. Several researchers deals with the synthesis and investigation

of different kinds of surfactants as corrosion inhibitors in acidic medium [36-43]. However, there is no published report on the corrosion inhibition effect of alginate surfactant derivatives for low carbon steel in HCl solution and electrochemical investigations highlighting the influence of alginate surfactant on kinetics of anodic and cathodic partial reactions of the corrosion process. Therefore, the present study was undertaken to assess the corrosion inhibition effect of alginate surfactant ant its metal complexes for carbon steel in 1 HCl solution using chemical and electrochemical techniques. The associated activation energy of corrosion and other thermodynamic parameters such as enthalpy, entropy of activation, adsorption–desorption equilibrium constant, standard free energy of adsorption, heat, and entropy of adsorption were calculated to elaborate the corrosion inhibition mechanism.

2. Experimental method

2.1. Materials

The corrosion measurements were performed on low carbon steel samples with the following composition (wt%): 11% C, 0.45% Mn, 0.04% P, 0.05% S, 0.25% Si, and the reminder is Fe. The mild steel coupons of 3.5 × 1.5 × 0.04 cm dimensions were used for the weight loss study. For the electrochemical studies, the specimens were covered with an epoxy resin leaving an exposed surface area of 1 cm^2 in aqueous solution. The specimens used for the analysis were polished with a series of emery paper (320–1200), washed with double-distilled water, degreased with acetone and dried at room temperature.

A commercially available alginic acid sodium salt, low viscosity, derived from (*Macrocystis pyrifera)* was purchased from Sigma Chemical Co., This had a peak relative molecular mass (RMM) of 344000, as determined by gel permeation chromatography (GPC), 2-(dimethylamino)ethanol (99%), 1-bromododecane (97%), cobalt chloride anhydrous (97%), copper chloride anhydrous (97%) and zinc chloride anhydrous (97%) of analytical grade were obtained from Aldrich Chemical Company (Germany). All the reagents were analytical grade and used as received. Organic solvents were purchased from commercial supplier and used without further purification.

2.2. Solutions

The corrosive solution was a 1.0 M hydrochloric acid solution diluted from concentrated acid (37%, Merck) with double-distilled water. This solution was used

as blank. Concentration range of used synthesized inhibitor varied from 5 x 10^{-5} to 5 x 10^{-3} M for corrosion measurements. All tests were performed in non-deareated solutions under unstirred conditions at 25, 45 and 60 ◦C.

2.3. Synthesis of inhibitors

2.3.1. *Synthesis of N-(2-hydroxyethyl)-N, N-dimethyldodecan-1-aminium bromide cationic surfactant*

Cationic surfactants were obtained by direct reaction between equimolar amounts of 1-bromododecane (0.1 mol.) and 2-(dimethylamino)ethanol (0.1 mol.) in 50 ml ethanol. The reaction mixture was refluxed for 8 h and left overnight for complete precipitation of the cationic surfactant. The products were filtered off and recrystallized three times from ethanol to produce the desired N-(2-hydroxyethyl)-N,N-dimethyldodecan-1-aminium bromide cationic surfactant (Step.2) [43]Fig. 1.

2.3.2. *Synthesis of alginate derived cationic surfactant*

N-(2-hydroxyethyl)-N,N-dimethyldodecan-1-aminium bromide (0.1 mol.) and alginic acid produced from hydrolysis of sodium alginate using hydrochloric acid (Step.1) (0.1 mol.) were esterified individually in xylene (50 ml) as the solvent under reflux conditions at 138 °C and 0.01% *p*-toluene sulphonic acid as dehydrating agent, until the a zeotropic amount of water (0.1 mol., 1.8 ml) was removed. Then the solvent was removed using vacuum rotary evaporator. The *p*-toluene sulphonic acid was extracted from the reaction medium using petroleum ether. Subsequent purification was done by means of vacuum distillation to remove the excess and residual materials [44].The product obtained was designated as (**AS**) in (Step.3), Fig. 1**.**

2.3.3. *Synthesis of alginate derived cationic surfactant and its metal complexes*

To a solution of the synthesized alginate derived cationic surfactant (**AS**) (0.01 mol.) in ethanol (100 ml), metal ion solution of anhydrous $CoCl_2$, $CuCl_2$ and $ZnCl_2$ (0.005 mol.) in ethanol (50 ml) was added separately and refluxed for 6 h. The reaction mixture was left overnight to complete the precipitation of the products. The products were filtered off and recrystallized twice from ethanol to obtain the crystalline products of the desired alginate surfactant metal complexes (AS-Co, AS-Cu and AS-Zn) in (Step.4) [45, 46] Fig.1.

2.4. Methods

2.4.1. FTIR studies

Fourier transform infrared (FTIR) spectra was recorded for the synthesized inhibitors on an ATI Mattson Infinity Series TM, Bench top 961 controlled by win first TM

V2.01 software (Egyptian Petroleum Research Institute ‘‘EPRI’’) at 25 °C. About 2 mg of sample with 100 mg of KBr was fully grinded and mixed. The mixed samples were pressed into pills with a compressor and prepared pellets were used for studies. All spectra were scanned against a blank KBr pellet back-ground in the range of 4000–400 $cm^{-1}$with resolution of 4.0 cm^{-1}.

2.4.2.^{1}H NMR studies

The ^{1}H-NMR was measured in DMSO-d_6 by Spect Varian, GEMINI 200 (^{1}H 200 MHz) (Micro-analytical Center, Cairo University). The synthesized inhibitors were dissolved in DMSO-d_6 solvent.

2.4.3. UV–vis studies

UV–Vis spectra of the synthesized inhibitors were carried out at 200–800 nm using a 3–5 mm quartz cuvette using UV–Vis Shimadzu, UV-2550, Japan. For the analysis, 5 ml of 2 mM aqueous solution of the synthesized alginate surfactant and its metal (II) complexes were put in a cuvette for measurement. All the measurements were carried out at room temperature.

2.4.4. Electrochemical methods

Electrochemical measurements were carried out using a Voltalab 40 Potentiostat PGZ 301 and a personal computer was used with Voltamaster 4 software at 25 ^oC and frequency response analyzer in a three-electrode arrangement. Carbon steel was taken as the working electrode, platinum as the counter electrode and saturated calomel electrode as reference electrode. The working electrode was held in the electrolyte solution for 60 min before each measurement for attaining a steady-state potential. For polarization studies, the potential was swept from cathodic direction to anodic direction with respect to open circuit potential (−1000 mV to +100 mV) at a scan rate of 1 mV/s. The point of intersection of extrapolated tafel lines gives the value of corrosion current density I_{corr} and corrosion potential E_{corr}. The inhibition efficiency is calculated using the corrosion current densities values in the absence and presence of various concentrations of the inhibitor. The electrochemical impedance spectroscopy (EIS) measurements were performed in the frequency range 100 kHz to 30 mHz, using AC signals of amplitude of 5 mV peak to peak. All the impedance values were measured at open circuit potential. Nyquist plot represents the results from EIS measurements. The charge transfer resistance (R_{ct}) and capacitance of double layer (C_{dl}) were calculated from the Nyquist plot [47].

2.4.5. Gravimetric method

Pre cleaned carbon steel samples in triplicate were weighed and immersed for 24 h in 100 ml of 1 M HCl without and with different concentrations of inhibitor. Experiments were performed in aerated condition at temperature 25, 45 and 60 °C and left unstirred. After immersion, the steel specimens were washed with double distilled water, dried and weighed again. The average weight loss is calculated. The inhibition efficiency is calculated for the synthesized inhibitors at each concentration [48].

2.4.6. Energy dispersive analysis of X-rays (EDAX)

EDX system attached with a Joel 5400 scanning electron microscope was used for elemental analysis or chemical characterization of the film formed on the steel surface. As a type of spectroscopy, it relies on the investigation of sample through interaction between electromagnetic radiation and the matter, so a detector was used to convert X-rays' energy into voltage signals. This information is sent to a pulse processor, which measures the signals.

2.4.7. Scanning electron microscope (SEM)

The CS specimens of size 7 cm x 3 cm x 0.5 cm were abraded with emery paper (grade 320–400–600–800–1000–1200) and gave a mirror surface, then washed with distilled water and acetone. After immersion in 1 M HCl without and with addition of 5 x 10^{-3} M of the synthesized alginate surfactants at 25 °C for 24 h, the specimens were cleaned with distilled water, dried with a cold air blaster, and then examined with SEM Jeol JSM-5400.

3. Results and Discussion

3.1. FTIR studies

Fig. 2 shows the FTIR spectra of AS, AS-Co, AS-Cu and AS- Zn. IR Spectra provide a lot of valuable information on coordination reaction. The IR spectra provide some important information regarding the skeleton of the complexes. In order to study the binding mode of the alginate surfactant to the metal in the complexes, the IR spectrum of the free ligand (alginate surfactant) was compared with the spectra of the complexes (Fig. 2). There were some minor differences between the metal (AS-Co, AS-Cu and AS-Zn) complexes and the free ligand (AS) upon chelation as expected. The IR spectra of the complexes show a sharp band in the range 3310–3493 cm^{-1}, attributed to ν(OH), which is shifted to higher frequency ongoing from the free ligand (at 3300 cm^{-1}) to the complexes. This is an indication of the coordination of the hydroxyl group to the metal. New bands of low intensity are observed in FT-IR region

in the range of 689-707 cm^{-1} which can be assigned to *v*(M-O) stretching vibrations [49]. On the other hand, the *v* (-C-O-), which occur at 1020 cm^{-1} for the ligand, was moved to higher frequencies, 1048–1080 cm^{-1} after complexation, this shift confirms the participation of phenolic oxygen of the ligand in complex formation. The bands present in the range 2910–2930, 283048-2860 cm^{-1} may be assigned to *v*(−C–H) stretching. The bands, in this ligand, due to $v((CH_2)_n)$ appear at 1450 cm^{-1}. These remain almost unchanged in the spectra of complexes, indicating that long alkyl chains are not participating in coordination [50]. In the free ligand, the sharp band observed at 1590 cm^{-1} is due to *v*(−CO). In all complexes, this band remains quite unchanged confirming the noninvolvement of the carbonyl ester in complex formation [51].

3. 2.^{1}H NMR studies

The ^{1}HNMR spectra of alginate ligand and its metal complexes were recorded to confirm the structure. The spectrum of alginate derivatives (Fig.3a-d) showed a weak singlet peak at δ = 0.88 and that are assigned to $–CH_3$ proton. This peak remains quite unchanged in the spectra of cobalt (II), copper (II) and zinc (II) complexes (Fig. 3) that confirming the noninvolvement of the methyl in complex formation. The singlet peak of –OH in the **AS** ligand (4.65 ppm) was shifted to higher values at 5.51, 5.05 and 5.41 ppm in cobalt (II), copper (II) and zinc (II) complexes, respectively, this confirm the participation of –OH group in the complexation. The higher value of the proton for the –OH group can be assigned to the presence of intermolecular hydrogen bonds. The group of peaks (m, nH, $(C\underline{H}_2)_n$) at δ = 1.23 – 1.81 ppm range are assigned to repeated methylene groups of the long alkyl chain and at δ = 1.65-2.61, 1.89-2.85, 2.35-3.05, 2.71-3.49 and 3.45-4.01 ppm for (t, 2H, $C\underline{H}_2N^+$), (m, 2H, $C\underline{H}_2CH_2N^+$), (m, 3H, $CH_2N^+(C\underline{H}_3)_2$),(t, 2H, $C\underline{H}_2N^+(CH_3)_2$), (t, 2H, $C\underline{H}_2CH_2N^+(CH_3)_2$), respectively [52]

3. 3. Ultraviolet Spectroscopy studies

UV-visible absorption spectra are very sensitive to the formation of metal complexes, due to metal complexes exhibit intense absorption peaks correspond to the bond formation between the metal ions and the ligands. Fig. 4 represents the UV-spectra of the synthesized alginate surfactant (AS) and alginate surfactant- metal complexes. The new absorption band is due to the electronic transition of *d*-orbitals of the different transition metal ions incorporated in the metal complexes. Further analysis of UV spectra revealed that the new absorption bands appeared at higher wavelengths

for larger diameter ions (e.g., Zn, ca. 220 nm, Cu, ca. 218 nm), while for the smaller ion, Co(II), the absorption band appeared at lower wavelength (212 nm). That indicates a higher energy is required for *d*-electrons transition in case of Co (II) ions, due to its small ionic radius. In case of Zn (II) and Cu(II), the ionic radii are larger and the energies required for *d*-electrons transition are less than that of Co(II). Additionally, UV absorption spectra confirmed the formation of the metal complexes of the cationic surfactants [53].

3.4. Potentiodynamic polarization measurements

The potentiodynamic polarization curves for carbon steel in 1.0 M HCl without and with different concentrations of alginate surfactants (AS) was shown in Fig. 5. (Polarization curves of AS-Zn, AS-Co, and AS-Cu, supplementary data file). As could be seen in the figure, both the cathodic and anodic (more pronounced on the cathodic) current densities decrease considerably on the introduction of alginate derivatives into the corrodent (1.0 M HCl). Also the corrosion potential (E_{corr}) in the presence of alginate derivatives is slightly displaced towards the negative direction compared to the blank solution. The cathodic polarization curves is also observed to give rise to parallel Tafel lines indicating that there is no modification of the hydrogen evolution reaction process on the introduction of alginate derivatives into the corrosive medium. This also suggests that alginate derivatives inhibits carbon steel corrosion by simply blocking the reaction sites without affecting the actual reaction mechanism [56]. Values of electrochemical parameters derived from the polarization measurements namely corrosion current density (I_{corr}), corrosion potential (E_{corr}), anodic (β_a) and cathodic (β_c) Tafel slopes, surface coverage and inhibition efficiency (η %) are listed in Table 1. Inhibition efficiency, (η_p, %), was obtained from the following equation [57]:

$$\eta_p\% = \left(\frac{i_{corr} - i^{\circ}_{corr}}{i_{corr}}\right) \times 100 \qquad (1)$$

where i_{corr} and i^{0}_{corr} are uninhibited and inhibited corrosion current densities, respectively, determined by extrapolation of Tafel lines to the corrosion potential.

Data in the Table 1 show that I_{corr} decreased in the presence of alginate derivatives compared to the blank solution and further decreases as the concentration of alginate derivatives increased. This is an indication that alginate derivatives inhibited the acid-induced corrosion of low carbon steel. Inspection of the Table 1 also reveals

noticeable changes in both the anodic and cathodic Tafel slopes. It is clear that the presence of the inhibitors causes a markedly decrease in the corrosion rate. The increase in inhibition efficiency is associated with a shift of both cathodic and anodic branches of the polarization curves towards lower current densities, together with a negative shift in $E_{corr,}$ suggest that the four inhibitors act as mixed type inhibitors with predominantly cathodic; i.e. meaning inhibitors reduce the anodic dissolution of mild steel and retards the cathodic hydrogen evolution reaction, but the effect on the cathodic hydrogen evolution reactions surface is more than the anodic dissolution reactions. Also the corrosion rate is observed to decrease in the presence of alginate derivatives in comparison to its absence indicating decreased metal dissolution and further decreases with increasing concentration. As also shown in Table 1, inhibition efficiency increased with increase in concentration of alginate derivatives reaching the maximum value of 95.51% at the concentration ($5x10^{-3}$ M) studied.

Interaction of transition metal complexes with mild steel is greatly affected by their standard electrode potentials, their reactivity and the nature of the ligand that could stabilize the metallic complexes. Standard electrode potential of divalent cations follows the order: Cu(II)/Cu (+0.34 V) > Co(II)/Co (−0.277 V) > Fe(II) > Fe (−0.44 V) > Zn(II)/Zn (-0.76 V). Reduction of Cu (II) and Co(II) species on the mild steel surface is possible due to their noble standard electrode potential compared to Fe(II). However, it should be noted that charged ligands could stabilize the higher oxidation states. Hence, the reduction of Cu (II) and Co(II) on the steel surface could be affected by the ligands surrounded them. Reduction of Cu (II) on steel could occur because of much more positive standard electrode potential of Cu(II)/Cu (+0.34 V SHE) compared to Fe(II)/Fe (−0.44 V SHE). Although charged ligands could stabilize the higher oxidation states, it seems that the change can not overcome the big difference between standard electrode potentials of Fe(II)/Fe and Cu(II)/Cu. Deposition of copper on the steel surface could lead to galvanic coupling which in turn results in decrease of charge transfer resistance and prevent carbon steel dissolution. The inhibition efficiency of the investigated inhibitors was increased in the following order: AS-Cu >AS-Co> AS-Zn >AS [58]. The uncertainties associated to the polarization experimental data for three replicates experiments is shown in Table (1).

3.5. Electrochemical impedance spectroscopy (EIS)

3.5.1. Nyquist plots

The impedance responses of low carbon steel in 1 M HCl in the absence and presence of alginate surfactant (AS) is depicted in Fig. 6. (Impedance curves of AS-Zn, AS-Co, and AS-Cu, supplementary data file). It could be observed from the Nyquist plots that the impedance responses of low carbon steel in the acid medium changed on addition of the inhibitor. The Nyquist plot is characterized by one semicircle capacitive loop corresponding to one time constant in the Bode plot suggesting that the corrosion of carbon steel is controlled by a charge transfer process. The diameter of the semicircles in the Nyquist plot and the magnitude of Bode modulus are observed to increase with increasing concentration of alginate derivatives indicating the formation of an adsorption film on the steel surface. In all cases, the Nyquist plot are not perfect semicircles but depressed with center under the real axis. These kinds of deviations are often referred to as the frequency dispersion of interfacial impedance [59]. The anomaly is usually attributed to the inhomogeneity of the electrode surface arising from surface roughness or interfacial phenomena [59]. The equivalent circuit (EC) model shown in supplementary data file was used to model the physical processes taking place at the steel /solution interface. The EC consists of solution resistance (*Rs*), charge transfer resistance (*Rct*) and constant phase element (*CPE*). The *CPE* is substituted for the capacitive element to give a more accurate fit as specified in the *CPE* impedance shown in the following equation:

$$Z_{CPE} = Q^{-1}(j\omega)^{-n} \qquad (2)$$

where *Q* and *n* stand for the *CPE* constant and exponent respectively, j = (–1) is an imaginary number and ω is the sine wave modulation angular frequency in rad s^{-1} ($\omega = 2\pi f$; where *f* is the frequency in Hz). The corresponding impedance parameters obtained are listed in Table 2. Data in the table show that alginate derivatives caused an increase in the R_{ct} value and a corresponding decrease in C_{dl}. Such an increase in the R_{ct} value, synonymous with an increase in the diameter of the semicircle in the Nyquist plot as well as the increase in the magnitude of the absolute impedance in the Bode plot point towards improved corrosion resistance due to the corrosion inhibiting action of alginate derivatives. The C_{dl} was computed using the expression [60]:

$$f_{max} = \frac{1}{2\pi C_{dl} R_{ct}} \qquad (3)$$

where f_{max} the frequency at which the imagiary component of the impedance is a maximum.

In case of the electrochemical impedance spectroscopy, the inhibition efficiency was calculated using charge transfer resistance according to the following equation [60]:

$$\eta_{\mathrm{I}} = \left(\frac{R_{\mathrm{ct}} - R^{\mathrm{o}}_{\mathrm{ct}}}{R^{\circ}_{\mathrm{ct}}} \right) \times 100 \qquad (4)$$

where R_{ct} and $R°_{ct}$ are the charge transfer resistance values without and with inhibitor for carbon steel in 1 M HCl, respectively.

The observed decrease in the values of C_{dl}, which normally arises from a decrease in the dielectric constant and/or an increase in the double-layer thickness, is as a result of adsorption of alginate derivatives onto the metal/electrolyte interface [61].

The uncertainties associated to the impedance experimental data for three replicates experiments is shown in Table (2).

3.5.2. Bode plots

For more complicated system, Bode plots can give more information. The Bode plots of the synthesized inhibitor (AS-Cu as representative inhibitor) are presented in Fig. (7). The low frequency impedance modulus Z_{mod} is one of the parameters which can be easily used to compare corrosion resistance of different samples. A larger Z_{mod} demonstrates a better protection performance [62].

In Fig. (7), it is shown that Z_{mod} increases as a function of the concentration of the synthesized inhibitor (AS-Cu). These phenomena can be explained as follows, the high frequency phase angle range (10^5–10^4 Hz) of the impedance spectra corresponds to the properties of an outer layer, the middle frequency range (10^4–10^2 Hz) reflects the properties of an inner barrier layer, while the low frequency range (less than 10^2 Hz) corresponds to the properties of the double-electrical layer information. Therefore, the high frequency phenomenon may due to the thickness increase of the outer porous layer, and the middle frequency phenomenon can be attributed to the penetration of active chloride ions and water through the defect of the prepared inhibitors inner barrier layer, though the whole effect induced the increase of Z_{mod}.

As seen from Fig. (7), Bode plots refer to the existence of an equivalent circuit that contains a single constant phase element in the metal/solution interface. The increase of absolute impedance at low frequencies in Bode plot confirmed the higher protection with increasing the concentration of the prepared inhibitors, which is related to adsorption of the inhibitors on the carbon steel surface [63].

The phase angle plots for the carbon steel in the presence and absence of synthesized inhibitors (AS-Cu as representative inhibitor) concentrations in 1.0 M HCl solution are given in Fig. (7). As seen from Fig. (7),the increasing of the inhibitors concentration in the test solution indicated superior inhibitive behavior due to adsorption of the metal surface of more prepared inhibitors molecules at higher concentrations. Furthermore, the depression of phase angle at relaxation frequency occurs with decreasing of inhibitors concentration which indicated the decrease of capacitive response with the decrease of inhibitors concentration. Such a phenomenon could be attributed to higher corrosion activity at low concentrations of inhibitors.

3.6. Weight loss measurements

3.6.1. Effect of inhibitor concentration

The corrosion rate (k) was calculated from the following equation [64]:

$$k = \frac{\Delta W}{St} \qquad (5)$$

where ΔW is the average weight loss of three parallel carbon steel sheets, S is the total area of one specimen, and t is immersion time.

The inhibition efficiency (η_w) of the prepared cationic surfactant inhibitors on the corrosion of CS are calculated from the following equation [65]:

$$\eta_w = \left(\frac{W_{corr} - W^o_{corr}}{W_{corr}}\right) \times 100 \qquad (6)$$

where W and W_o are the weight loss of carbon steel in the absence and presence of the inhibitors, respectively.

The inhibition efficiency values of CS with different concentrations of the synthesized inhibitors in 1.0 M HCl solution at 25 ^oC was shown in supplementary data file (Fig.8). The inhibition efficiency values increase as the concentration of the inhibitor increases, i.e. the corrosion inhibition enhances with the inhibitor concentration. This behavior is due to the fact that the adsorption coverage of inhibitor on CS surface increases with the inhibitor concentration.

3.6.2. Effect of complexation on the inhibition efficiency

Increase the corrosion inhibition efficiency by complexation. That could be due to the increase in the hydrophobicity of these complexes in comparison to the parent alginate surfactant, which is due to the presence of two ligands coordinated to the metal ion within the giant structure of the complex containing a methylene group, i.e., more non-polar chains. Then the water/surfactant molecules interactions increased,

which forced them to the air water interface [66]. In fact, these results suggest that, two alkyl chains in one molecule linked by a metal ion enhance the adsorption and aggregation properties, by strengthening the inter- or intra-molecular hydrophobic interaction. The higher number of uniqueness of the metal–surfactant coordination complexes lies in the fact that the bond between the head group and the tail part of the surfactant is a coordinate bond and the surfactant contains a higher charge on the head group which leads to more repulsion in the bulk of aqueous solution and increasing adsorption onto the carbon steel surface.

The inhibition efficiency results in Table 3 reveal that the efficiency was increased by increasing electronegativity of the transition metal. The inhibition efficiency was increased in the following sequence: $Cu^{+2} > Co^{+2} > Zn^{+2}$ because the electronegativity of this transition metal as the following: (Cu^{+2} = 1.90, Co^{+2} = 1.88 and Zn^{+2} = 1.65). This can be explained by the electronegativity of these ions, which increases their attraction for the metal surface; hence their complexes with the ligands will be polar in nature. The polarity will increase the adsorption of these metallo compounds on the carbon steel surface and consequently increase the inhibition efficiency [58].

3.6.3. Effect of temperature

Temperature plays an important role in the progress of corrosion reactions of metal in acid media. It is sometimes used as a gauge to determine whether an inhibitor is physically or chemically adsorbed on a metal surface to inhibit corrosion; as increase in inhibition efficiency with increase in temperature is often associated with chemisorption phenomenon while the reverse signifies physisorption. To assess the effect of temperature on the corrosion and corrosion inhibition of carbon steel without and with alginate derivatives, weight loss experiments were undertaken at 25, 45 and 60 ^{o}C using different concentration of inhibitors. The results obtained for 24 h immersion period is presented in Table 3 and show that corrosion rates of carbon steel in 1 M HCl in the absence and presence alginate derivatives decreased with increase temperature. Further inspection of Fig. 9 (supplementary data file) reveals that inhibition efficiency increased with increase in temperature. For instance, at 25 ^{o}C, the values of inhibition efficiency obtained at 5x 10^{-5} and 5x 10^{-3} M for (AS-Cu) were 69.9 and 93.7% respectively. As the temperature was raised to 60 ^{o}C, the η% was increased to 79.5 and 96.1% respectively. Data revealed that the inhibition efficiency increased with increasing temperature, indicating that the inhibitor was

more effective at higher temperature up to 60 ^{o}C. This could be explained by chemisorption of adsorbed inhibitor on the carbon steel surface.

The uncertainties associated to the weight loss experimental data for three replicates experiments is shown in Table (3).

3.6.4. Effect of the exposure time in the corrosive media

It has been shown that the inhibiting ability of organic molecules strictly depends on exposure time in the aggressive solutions [67]. To assess the retarding behavior of corrosion inhibitors on a time scale, weight loss measurements were carried out in 1 M HCl solution in absence and in presence of the synthesized inhibitors (AS, AS-Zn, AS-Co and AS-Cu) at $5x10^{-3}$ M for different exposure time (24, 50, 100, 200 and 300 h) at 25 ^{o}C. Inhibition efficiencies calculated from equation (6) were plotted against immersion time as seen in Fig.8. It is clear that the inhibition efficiencies of the different inhibitors are gradually decreased by increasing the immersion time and the maximum inhibition efficiency values after 24 h of immersion in inhibited solutions. The increase in inhibition efficiencies after 24 h for the tested inhibitors reflects their strong adsorption on the carbon steel surface, which results a more protective layer. The high inhibition efficiency after 24 h can be attributed to the formation of a protective film is time-dependent on the steel surface. It has been stated that stable, two-dimensional layers of inhibitor molecules are formed on metal surfaces after immersion time 24 h.

Fig. 8. it is possible to note that inhibition efficiency diminishes linearly up to 200 h, though after this time it remains practically constant. This is because the increase of immersion time increases the values of anodic current, and cathodic current, while decreases the surface and polarization resistances, which reflects on the increase of the corrosion rate with time, the obtained results are similar to published data [68].

3.7. Adsorption isotherm

Different adsorption isotherm models were assessed in order to determine the nature of interaction between alginate derivatives and carbon steel surface. The value of correlation coefficient (R^2) was used to determine the best fit adsorption isotherm that best described the adsorption of alginate derivatives onto the steel surface. Best result was obtained with Langmuir isotherm (R^2 closed to 1). The construction of the isotherm was made possible by the degree of surface coverage (θ) determined from the following equation [65]:

$$\theta = \left(\frac{W_{\text{corr}} - W^{\circ}_{\text{corr}}}{W_{\text{corr}}}\right) \qquad (7)$$

where W_{corr} and W^{o}_{corr} are weight loss without and with inhibitor, respectively.

The equation that fits our results is that due to Langmuir isotherm and is given by the general equation [69]:

$$\frac{C}{\theta} = \left(\frac{1}{K_{ads}}\right) + C \qquad (8)$$

where C is the inhibitor concentration, K_{ads} is the adsorptive equilibrium constant and $\boldsymbol{\theta}$ is the surface coverage.

The surface coverage (θ) was tested graphically for fitting a suitable adsorption isotherm as indicated in Fig. 9. Plotting C/θ vs. C yielded a straight line with a correlation coefficient (r^2) equal to 1 as seen in Table 4. This indicates that the adsorption of these inhibitors can be fitted to a Langmuir adsorption isotherm. The strong correlation of the Langmuir adsorption isotherm may confirm the validity of this approach.

The slight deviation of slope obtained from the Langmuir isotherm plot from unity indicates that a monolayer inhibitor film is not formed on the steel surface and there are interactions between the adsorbed inhibitor molecules (deviation from ideal Langmuir postulates). This is not surprising given the fact that alginate are macromolecules with multiple adsorption centers/sites that may adsorbed differently on the metal surface. Such adsorbed species may interact by mutual repulsion or attraction. Similar observations have been reported in previous studies on adsorption and corrosion inhibition of chitosan, gum arabic and carboxymethyl cellulose (biopolymers) for mild steel in acid media [24,26,32].

The equilibrium constant (K_{ads}) for the adsorption–desorption process of these compounds can be calculated from reciprocal of the intercept. The adsorptive equilibrium constant (K_{ads}) values are listed in Table 4. It is clear that, the large values indicate a strong adsorption of the synthesized inhibitors on the surface of carbon steel in 1 M HCl at relatively higher temperatures. This may be due to the formation of coordinated bonds between the prepared cationic surfactants and the d-orbital of iron on the surface of steel. K_{ads} values usually indicate adsorption strength of the a dsorbate on the adsorbent. The relatively low value obtained at 25 ^{o}C is suggestive of

weak adsorption of the inhibitor on the metal surface; hence low inhibition efficiency at this temperature.

3.8. Thermodynamic parameters

The standard adsorption free energy (ΔG^0_{ads}) can be obtained according to the following equation [70-72]:

$$\Delta G^{\circ}_{\text{ads}} = -RT\ln(55.5\, K_{\text{ads}}) \qquad (9)$$

where R is the gas constant (8.314 J mol^{-1} K^{-1}), T is the absolute temperature, and the value 55.5 is the concentration of water in solution expressed in M.

The negative values of $\boldsymbol{\Delta G^0_{ads}}$ indicate that the adsorption of inhibitor molecule onto steel surface is a spontaneous process. Generally values of $\boldsymbol{\Delta G^0_{ads}}$ up to are 20 k J mol^{-1} consistent with the electrostatic interaction between the charged molecules and the charged metal (physical adsorption) while those more negative than - 40kJ mol^{-1} involve sharing or transfer of electrons from the inhibitor molecules to the metal surface to form a co-ordinate type of bond (chemisorption) [73–75]. Calculated $\boldsymbol{\Delta G^0_{ads}}$ values indicated that the adsorption mechanism of the prepared inhibitors on carbon steel in 1 M HCl solution is a chemical adsorption [76].

The adsorption heat can be calculated according to the Van't Hoff equation [77]:

$$\ln K_{ads} = \left(\frac{-\Delta H^{\circ}_{\text{ads}}}{RT}\right) + \text{constant} \qquad (9)$$

where ΔH^0_{ads} and K_{ads} are the adsorption heat and adsorptive equilibrium constant, respectively.

To obtain the standard enthalpy, plotting ln K_{ads} vs. 1/T (Fig. 10) yielded straight line according to Eq. (9) with slope equal -$\Delta H^o_{ads}/R$. The ΔH^0_{ads} values were equal to 3.3, 1.9, 5.1 and 3.3 kJ mol^{-1} for AS, AS-Zn, AS-Co and AS-Cu, respectively. The positive values of ΔH^0_{ads} indicated that the adsorption of investigated inhibitors on the carbon steel surface is endothermic.

Entropy of inhibitor adsorption ΔS^o_{ads} can be calculated using the following equation [78]:

$$\Delta G^{\circ}_{\text{ads}} = \Delta H^{\circ}_{\text{ads}} - T\Delta S^{\circ}_{\text{ads}} \qquad (10)$$

The obtained ΔS^0_{ads} values were listed in Table 4. The positive values of ΔS^0_{ads} mean that the adsorption process is accompanied by an increase in entropy, as was expected, since the endothermic adsorption process is always accompanied by an

increase of entropy which is the driving force for the adsorption of inhibitor onto the carbon steel surface [79].

3.9. Activation parameters

The apparent activation energy, E_a, of the corrosion reaction was determined using Arrhenius plots. Arrhenius equation could be written as [80]:

$$k = \mathrm{A}\exp\left(\frac{-E_a}{RT}\right) \qquad (11)$$

where E_a represents the apparent activation energy, R is the gas constant, T is the absolute temperature, A is the pre-exponential factor, and k is the corrosion rate.

The apparent activation energy of the corrosion reaction in the presence and absence of the inhibitor could be determined by plotting ln k against $1/T$, which gives a straight line with a slope permitting the determination of E_a. Fig. 11 shows these plots in the absence and presence of different concentrations of inhibitor (AS-Cu). The calculated values of the apparent activation corrosion energies in the absence and presence of inhibitors are listed in Table 5. The lower activation energy values in the presence of inhibitors support the results obtained from the weight loss and indicate the chemisorption of the inhibitors [81] .

Eq. (11) showed that, $-E_a/R$ is the slope of the straight line (ln k vs. $1/T$), so the value of E_a could elucidate the effect of temperature on corrosion inhibition. This behavior is indicated that the adsorption of the inhibitors on the carbon steel in 1 M HCl is chemisorption.

Enthalpy and entropy of activation (ΔH^*, ΔS^*) were calculated from the transition state theory [82] and listed in Table 5.

$$\ln\left(\frac{k}{T}\right) = \left(\ln\left(\frac{R}{N_A h}\right) + \left(\frac{\Delta S^*}{R}\right)\right) - \frac{\Delta H^*}{RT} \qquad (12)$$

where h is Planck's constant, N_A is Avogadro's number, R is the universal gas constant, ΔH^* is the enthalpy of the activation and ΔS^* is the entropy of activation. Plotting of ln (k/T) against $1/T$, (Eq. (12)), for carbon steel dissolution in 1 M HCl in the absence and presence of different concentrations from the synthesized inhibitors, gave straight lines as illustrated in Fig. 21. Data in Table 5 represented the values of ΔH^* and ΔS^*, which were calculated from the slope of - $\Delta H^*/R$ and the intercept of ($\ln(R/N_A h) + \Delta S^*/R$) of the straight lines. Values of ΔH^* and ΔS^* were calculated and listed in Table 5. Inspection of these data revealed that the positive signs of the

enthalpy (ΔH^*) reflected the endothermic nature of the steel dissolution process and indicated that the dissolution of steel was difficult [83]. It is clear that from Table 5 ΔS^* values in the absence and presence of the prepared alginate derivatives have negative sign, This implies that the activated complex in the rate-determining step represents an association rather than dissociation, indicating that more order takes place, going from reactant to activate complex [84]. The values of entropy of activation ΔS* in tested solutions are large and negative. The table illustrates that values of ΔS* move towards more negatives values with increasing inhibitor molecular weight. However many authors have discussed this phenomenon. As in the free acid solutions, the transition state of the rate determining recombination step represents a more orderly arrangement relative to the initial state. Hence, a large negative value for the entropy of activation is obtained. In the presence of the inhibitors, the rate-determining step is the discharge of hydrogen ions to form adsorbed hydrogen atoms. The discharge of hydrogen ions at the metal surface will be retarded by adsorption of inhibitor molecules on the surface metal. This causes the system passes from a more orderly to a less orderly arrangement, and hence the less negatives values of activation entropy is observed.

3.10. Energy dispersive X-ray analysis (EDX)

EDX micrographs of the surfaces of carbon steel were recorded in order to see the changes occurred during corrosion process in the absence and presence of the inhibitors as shown in (supplementary data file, Figs (10a,b). The EDX spectrum of carbon steel in uninhibited 1.0 M HCl (supplementary data file, Fig. 10a) showed the characteristic peaks of the elements constituting carbon steel sample which showed the oxide film formed (8.4 %). However, EDX spectrum of inhibited carbon steel (supplementary data file, Fig. 10b) in presence of $5x10^{-3}$ M of the synthesized alginate surfactant (AS-Cu) showed the oxide percentage (-0.64). These indicated that the surfaces were covered with protective film of the inhibitors molecules. The inhibitors molecules were strongly adsorbed on the carbon steel surface.

3.11. Scanning Electron Microscopy (SEM)

The SEM micrographs of the corroded carbon steel in the presence of 1 M HCl solution are shown in (supplementary data file, Fig. 11a). The faceting seen in this figure was a result of pits formed due to the exposure of carbon steel to the acid. The influence of the inhibitor addition (5×10^{-3} M) on the carbon steel in 1 M HCl solution is shown in (supplementary data file, Fig. 11b). The faceting observed in figures disappeared and the surface was free from pits and it was smooth. It can be

concluded from (supplementary data file, Fig. 11b) that corrosion does not occur in presence of inhibitor and hence corrosion was inhibited strongly when the inhibitor was present in the hydrochloric acid.

3.12. Mechanism of inhibition

Results obtained from all the experimental techniques reveal that addition of alginate derivatives to the acid corrosive medium retarded the corrosion of carbon steel. The corrosion inhibition process no doubt occurs by virtue of adsorption mechanism where the oxygen and nitrogen heteroatoms present in alginate molecular structure serves as adsorption centers to contain excessive negative charges. The thermodynamic data suggests that the adsorption of alginate derivatives on the steel surface follows chemisorption mode at higher temperature. In acidic medium, the anodic dissolution of iron is accompanied by the cathodic hydrogen evolution reaction as follows:

$$\mathbf{Fe \rightarrow Fe^{2+} + 2e^{-}} \qquad \mathbf{(13)}$$

$$\mathbf{2H^{+} + 2e^{-} \rightarrow H_2\uparrow} \qquad \mathbf{(14)}$$

Potentiodynamic polarization results indicate that alginate derivatives follow mixed inhibition mechanism. The chemical structure of alginate derivatives repeat unit (Fig.1) reveals the presence of ammonium–N^{+}, –$COOCH_2CH_2$ and –OH functional groups. It could be assumed that the cationic form of alginate may be adsorb on the cathodic sites of carbon steel and inhibits the cathodic hydrogen evolution reaction. On the other hand, –OH groups have lone pairs of electrons and can be adsorbed on the anodic sites of the metal surface via interaction with the vacant d-orbital of iron and inhibits the anodic metal dissolution reaction. These processes effectively help in isolating the metal surface from the aggressive ions present in the acid medium and thereby inhibiting corrosion. It is also known that in the acid corrosive medium, the inhibitor (alginate derivatives) may be protonated and exists as polycation and the surface of Fe is positively charged hence occurrence of mutual repulsion between them. However, the specific adsorption of chlorides ions (Cl^{-}) and replacing hydroxyl groups on the metal surface would render the metal surface negatively charged and surface activity of surfactants[27, 85-89]. Hence alginate in the form of polycation will be adsorbed on negatively charged metal surface and inhibit corrosion.

4. Conclusions

Electrochemical and chemical techniques of monitoring corrosion as well as surface

analysis approach were employed to evaluate the potential of alginate derivatives (a biopolymer) as an inhibitor for carbon steel corrosion in acidic environment. Results obtained show that alginate derivatives act as good inhibitor for acid-induced corrosion of carbon steel. Corrosion inhibition effect was found to be inhibitor concentration and temperature dependent; inhibition efficiency increased with increasing alginate derivatives concentration and solution temperature. Potentiodynamic polarization studies reveal that alginate derivatives functions as a mixed-type inhibitor but under cathodic control. Alginate derivatives are assumed to function as an inhibitor by virtue of adsorption of its molecules onto the steel surface which can be approximated by Langmuir adsorption isotherm model. The results obtained from the weight loss measurements were in good agreement with those obtained from the potentiodynamic polarization and EIS methods.

5. Reference

1. A.M. Al-Sabagh , H.M. Abd-El-Bary, R.A. El-Ghazawy , M.R. Mishrif, B.M. Hussein, Egyptian Journal of Petroleum 20 (2011) 33–45

[2] M.A. Migahed, M. Abd-El-Raouf, A.M. Al-Sabagh, H.M. Abd-El-Bary, Electrochim. Acta 50 (24) (2005) 4683–4689

[3] E.E. Oguzie, S.G. Wang, Y. Li, F.H. Wang, J. Phys. Chem. C 113 (2009)8420.

[4] R. Uffana, S.M. Ashraf, S. Ahmad, Prog. Org. Coat. 59 (2007) 138.

[5] A.K. Satapathy, G. Gunasekaran, S.C. Sahoo, K. Amit, P.V. Rodrigues, Corros. Sci.51 (2009) 2848–2856.

[6] P.C. Okafor, M.E. Ikpi, I.E. Uwah, E.E. Ebenso, U.J. Ekpe, S.A. Umoren, Corros. Sci.50 (2008) 2310–2317.

[7] A. Bouyanzer, B. Hommouti, Pigm. Resin. Technol. 33 (2004) 287–292.

[8] A. Chetouani, B. Hommouti, M. Benkaddour, Pigm. Resin. Technol. 33 (2004)26.

[9] A. Singh, V.K. Singh, M.A. Quraishi, J. Mater. Environ. Sci. 1 (2010) 162–174.

[10] S.K. Gopal Ji, P. Shukla, S. Dwivedi, E.E. Sundaram, R. Ebenso, Prakash, Int. J.Electrochem. Sci. 7 (2012) 12146–12158.

[1] M.A. Quraishi, I.H. Farooqi, P.A. Saini, Corrosion 55 (1999) 493–497.

[12] T.H. Ibrahim, Y. Chehade, M.A. Zour, Int. J. Electrochem. Sci. 6 (2011) 6542–6556

[13] T. Ibhrahim, M. Habbab, Int. J. Electrochem. Sci. 6 (2011) 5357–5371.

[14] A. Altwaiq, S. Khouri, S. Al-luaibi, R. Lehmann, H. Driicker, C. Vogt, J. Mater.Environ. Sci. 2 (2011) 259–270.

[15] F.S. de Souza, A. Spinelli, Corros. Sci. 51 (2009) 642–649.

[16] B. Qian, J. Wang, M. Zheng, B. Hou, Corros. Sci. 75 (2013) 184–192.

[17] V. Rajeswari, D. Kesavan, M. Gopiraman, P. Viswanathamurthi, Carbohyd.Polym. 95 (2013) 288–294.

[18] E. Bayol, A.A. Gvrten, M. Dursun, K. Kayakirilmaz, Acta Physico-Chim. Sin. 24(2008) 2236–2242.

[19] J. Fu, S.Li, Y.Wang, X.Liu, L.Lu, Journal of Materials Science 46(10), (2011)3550-3559.

[20] J.Fu, H.Zang, Y.Wang, S.Li, T.Chen, X.Liu., Industrial and Engineering Chemistry Research 51(18) (2012)6377-6386.

[21] G.Gece, Corrosion Science 53(12), (2011)3873-3898.

[22] A. R.Hosein Zadeh, I.Danaee, M. H. Maddahy, Journal of Materials Science & Technology 29(9), (2013)884-892.

[23] P.Roy, A.Pal, D.Sukul, RSC Advances 4(21), (2014) 10607-10613.

[24] M. M. Solomon, S. A. Umoren, I. I.Udosoro, A. P.Udoh, Corrosion Science, 52(4), (2010)1317-1325

[25] S. A.Umoren, M. J.Banera, T.Alonso-Garcia, C. A.Gervasi, M. V. Mirífico, Cellulose, 20(5), (2013) 2529-2545.

[26] S. A.Umoren, Z. M.Gasem, I. B. Obot, Industrial and Engineering Chemistry Research, 52(42), (2013)14855-14865.

[27] M. N. El-Haddad, A. S. Fouda, Journal of Dispersion Science and Technology, 34(10), (2013) 1471-1480.

[28] M. M.Hussein, M. El-Hady, H. H.Shehata, M.Hegazy, H. H. Hefni, Journal of Surfactants and Detergents, 16(2), (2013) 233-242.

[29] A. M. Alsabagh , M. Z. Elsabee , Y. M. Moustafa , A. Elfky , R. E. Morsi, Egyptian Journal of Petroleum 23 (2014)349–359

[30] V.Rajeswari, D.Kesavan, M. Gopiraman, P. Viswanathamurthi, Carbohydrate Polymers, 95(1), (2013) 288-294.

[31] H.Bentrah, Y.Rahali, A.Chala, Corrosion Science 82(0), (2014)426-431.

[32] S. A. Umoren, Cellulose, 15(5), (2008)751-761.

[33] S. A. Umoren, I. B.Obot, E. E.Ebenso, P. C.Okafor, O. Ogbobe, E. E. Oguzie, Anti-Corrosion Methods and Materials 53(5), (2006) 277-282.

[34] M.Bello, N.Ochoa, V.Balsamo, F.López-Carrasquero, S.Coll, A.Monsalve, G.González, Carbohydrate Polymers, 82(3), (2010) 561-568.

[35] I. Braccini, S. Pérez, Biomacromolecules 2 (2001)1089-1096.

[36] N.A.Negm, F.M. Ghuiba, S.A. Mahmoud, S.M.Tawfik, Eng. Life Sci. 11(5) (2011)496-510.

[37] N.A.Negm, Y.M.Elkholy, M.K.Zahran, S. M. Tawfik, Corrosion Science 52 (2010) 3523–3536.

[38] S. M. Tawfik, A.Sayed, I. Aiad, J Surfact Deterg. 15 (2012) 577.

[39] A.Abd-Elaal, I.Aiad, S. M. Shaban, S. M. Tawfik,. A.Sayed, Journal of Surfactants and Detergents 17 (2014) 483-491.

[40] N.A.Negm, F.M.Ghuiba, S. M. Tawfik, Corrosion Science 53 (2011) 3566–3575.

[41] I.Aiad, S. M.Tawfik, S. M.Shaban, A.Abd-Elaal, M.El-Shafie, Journal of Surfactants and Detergents17 (2014)391-401.

[42] S. M. Shaban, A.Sayed, S. M.Tawfik, A.Abd-Elaal, I. Aiad, Journal of Industrial and Engineering Chemistry 19 (2013) 2004.

[43] S. M. Tawfik , Journal of Molecular Liquids 209 (2015) 320–326.

[44] N.A.Negm, Y.M.Elkholy, F.M.Ghuiba, M.K.Zahran, S.A.Mahmoud, S.M.Tawfik, J Adsorp Sci Technol. 32 (2011)512-518.

[45] S. M. Tawfik, M. F. Zaky, J Surfact Deterg. 18 (2015) 863–871.

[46] M. F. Zaki, I. A. Aiad, S. M. Tawfik, Journal of Industrial and Engineering Chemistry 21 (2015)1174-1182.

[47] N. A. Negm, S. M. Tawfik, E. A. Badr, M. I. Abdou, F. M. Ghuiba, J Surfact Deterg 18 (2015) 413–420.

[48]N.A. Negm, F.M. Ghuiba, S. M. Tawfik, Corrosion Science 53 (2011) 3566–3575

[49] M. H. M. Hussein, M. F. El Hady, W. M. Sayed, and H. Hefni, Ser. A, 54 (2012)113–124.

[50] A.M.A. Alaghaz, H.A. Bayoumi, Y.A. Ammar, S.A. Aldhlmani, Molecu. Struct.1035 (2013) 383–399.

[51] M. Hwang, L. Lin, and W. Hwang, Progress In Electromagnetics Research Symposium Proceedings, Taipei, 28 (2013)372-375

[52] T. A. davis, F. llanes, B. volesky, G. diaz-pulido, L. mccook, A. mucc, Applied Biochemistry and Biotechnology 110(2003) 75-90.

[53] A.S. El-Tabl, R.M. El-Bahnasawy, M.M.E. Shakdofa, A.E. Abdalah, J. Chem. Res. 88 (2010) 210.

[54] A. A.Farag, M. A. Hegazy, Corrosion Science, 74(0), (2013)168-177.

[55] X.He, Y.Jiang, C.Li, W.Wang, B.Hou, L.Wu, Corrosion Science, 83(0), (2014) 124-136

[56] J.Hu, D.Zeng, Z.Zhang, T.Shi, G. L.Song, X.Guo, Corrosion Science, 74(0), (2013) 35-43.

[57] S. Haruyama, T. Tsuru, B. Gijutsu, J. Jpn. Soc. Corros. Eng. 27 (1978) 573.

[58] S. M. Tawfik, M. F. Zaky, Res Chem Intermed,DOI 10.1007/s11164-015-1926-4

[59] S.Martinez, M. Metikoš-Huković, Journal of Applied Electrochemistry,635 33(12), (2003) 1137-1142.

[60] S. M. Tawfik, A. A. Abd-Elaal,I. Aiad, Res Chem Intermed DOI 10.1007/s11164-015-2076-4.

[61] S. A.Umoren, M. M.Solomon, U. M.Eduok, I. B.Obot, A. U. Israel, Journal of Environmental Chemical Engineering, *2*(2), (2014)1048-1060.

[62] M.A. Hegazy, Ali M. Hasan, M.M. Emara, Mostafa F. Bakr, Ahmed H. Youssef, Corros. Sci. 65 (2012) 67–76.

[63] H. Keles, M. Keles, I. Dehri, O. Serindag, Mater. Chem. Phys. 112 (2008) 173–179.

[64] S. M. Tawfik, Journal of Molecular Liquids 207(2015) 185-194.

[65] O.K. Abiola, J.O.E. Otaigbe, Corros. Sci. 51 (2009) 2790.

[66] S. Ghareba, S. Omanovic, Corros. Sci. 52 (2010) 2104

[67] E.E. Oguzie, C. Unaegbu, C.N. Ogukwe, B.N. Okolue, A.I. Onuchukwu, Mater. Chem.Phys. 84 (2004) 363–368.

[68] X. Li, S. Deng, H. Fu, Corros. Sci. 53 (2011) 3241–3247.

[69] M. Palomar-Pardavé , M. Romero-Romo , H. Herrera-Hernández , M.A. Abreu-Quijano , Natalya V. Likhanova , J. Uruchurtu , J.M. Juárez-García, Corrosion Science 54 (2012) 231–243

[70] S.M. Tawfik , N. A. Negm, Res Chem Intermed (2015): DOI 10.1007/s11164-015-2233-9

[71] G. Moretti, F. Guidi, G. Grion, Corros. Sci. 46 (2004) 387.

[72] S.M.A. Hosseini, A. Azimi, Corros. Sci. 51 (2009) 728.

[73] F. Bentiss, M. Lebrini, M. Lagrenee, Corros. Sci. 47 (2005) 2915–2931.

[74] W.H. Li, Q. He, S.T. Zhang, C.L. Pei, B.R. Hou, J. Appl. Electrochem. 38 (2008) 289–295.

[75] E. Bensajjay, S. Alehyen, M. El Achouri, S. Kertit, Anti-Corros. Meth. Mater. 50 (2003) 402–409.

[76] N. A. Negm, E.A. Badr, S. M. Tawfik, A. F. El Farargy, Journal of Applied Chemistry, 7(6) (2014) 13.

[77] T.P. Zhao, G.N. Mu, Corros. Sci. 41 (1999) 1937.

[78] A.M. Badawi, M.A. Hegazy, A.A. El-Sawy, H.M. Ahmed, W.M. Kamel, Mater. Chem. Phys. 124 (2010) 458–465.

[79] H. Ashassi-Sorkhabi, B. Shaabani, D. Seifzadeh, Appl. Surf. Sci. 239 (2005) 154–164.

[80] M.M. Saleh, Mater. Chem. Phys. 98 (2006) 83–89.

[81] A. Popova, M. Christov, A. Vasilev, Corros. Sci. 49 (2007) 3276–3289.

[82] H. Ashassi-Sorkhabi, B. Shaabani, D. Seifzadeh, Electrochim. Acta 50 (2005) 3446–3452.

[83] M.S. Morad, A.M. Kamal El-Dean, Corros. Sci. 48 (2006) 3398–3412.

[84] A.S. Fouda, A.A. Al-Sarawy, E.E. El-Katori, Desalination 201 (2006) 1–13.

[85] N. A. Negm, S. M. Tawfik, M. I. Abdou, E. A. Badr, F. M. Ghuiba, Journal of Surfactants and Detergents, 18(2015)309-319

[86] S. M. Tawfik, Journal of Industrial and Engineering Chemistry 28 (2015) 171.

[87] M. F. Zaki, S. M. Tawfik. Journal of Oleo Science 63 (2014) 921. .

[88] G. H.Sayed, F. M.Ghuiba, M. I. Abdou, E. A.Badr, S. M.Tawfik, N. A. Negm, Colloids and Surfaces A: Physicochem. Eng. Aspects 393 (2012)96.

[89] R.Yıldız, T. Doğan, İ.Dehri, Corrosion Science 85 (2014) 215-221.

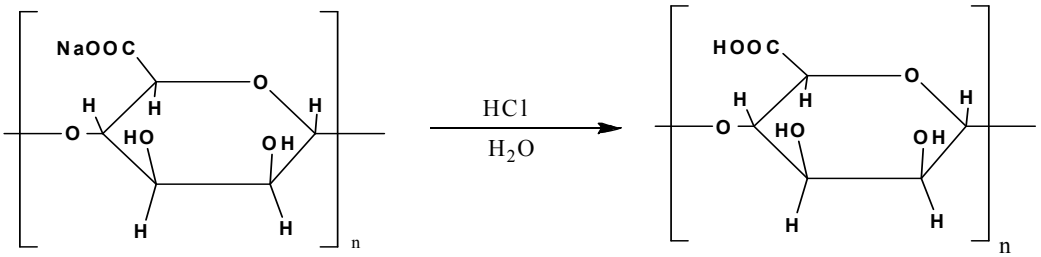

Sodium Alginate **Alginic acid**

Step. 2

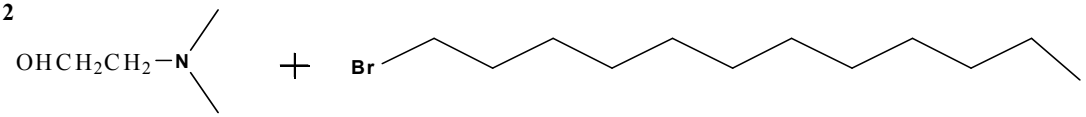

2-(dimethylamino)ethanol

Reflux **Ethanol**

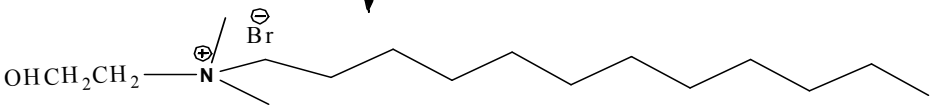

***N*-(2-hydroxyethyl)-*N*,*N*-dimethyldodecan-1-aminium bromide**

Step. 3

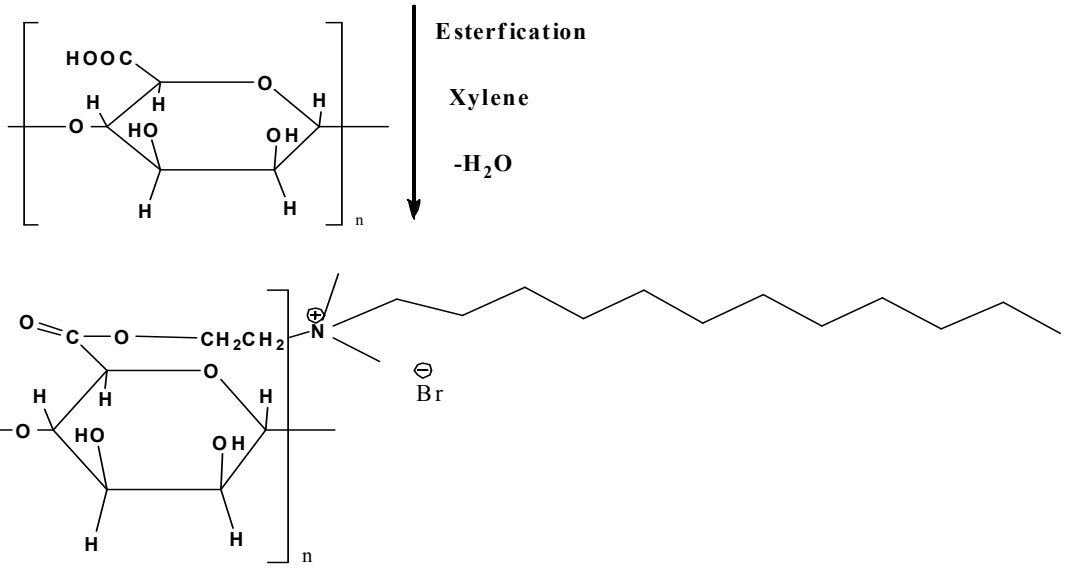

Alginate Surfactant (AS)

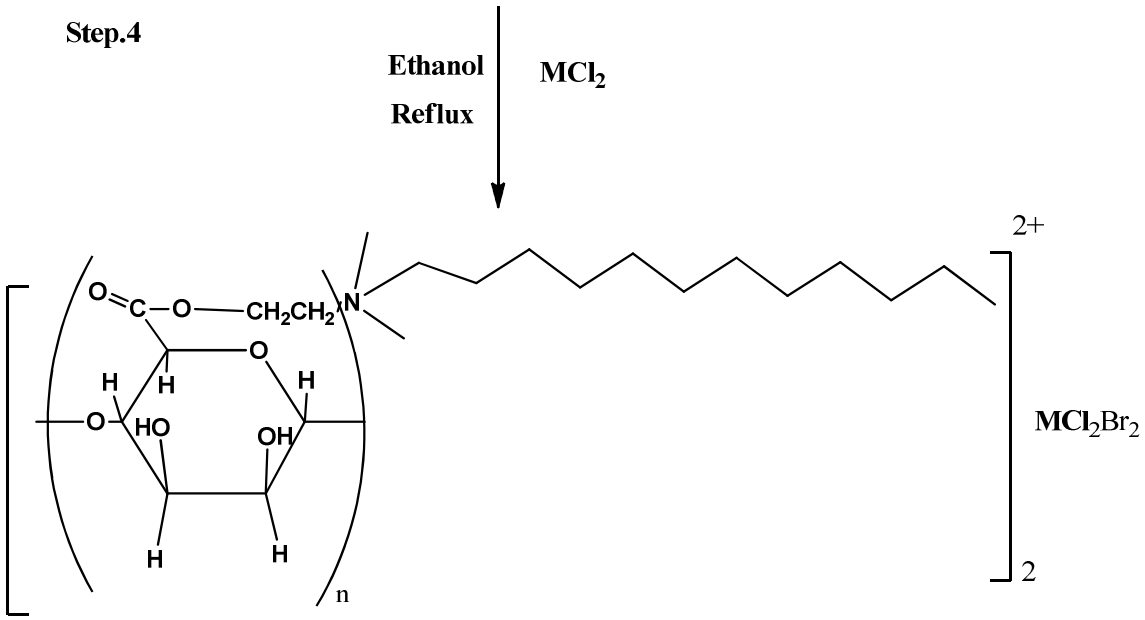

M= CO (AS-CO), Cu (AS-Cu), and Zn (AS-Zn)

Fig. 1. The chemical structure of the synthesized alginate cationic surfactant and its metal complexes

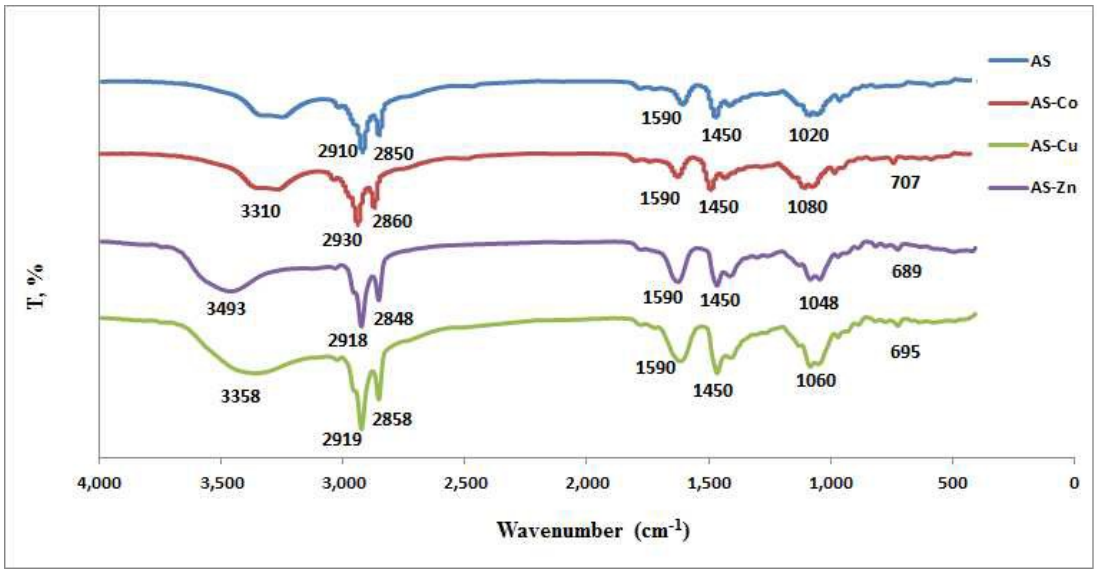

Fig. 2. FTIR spectra of the synthesized alginate derived cationic surfactant and its metal complexes

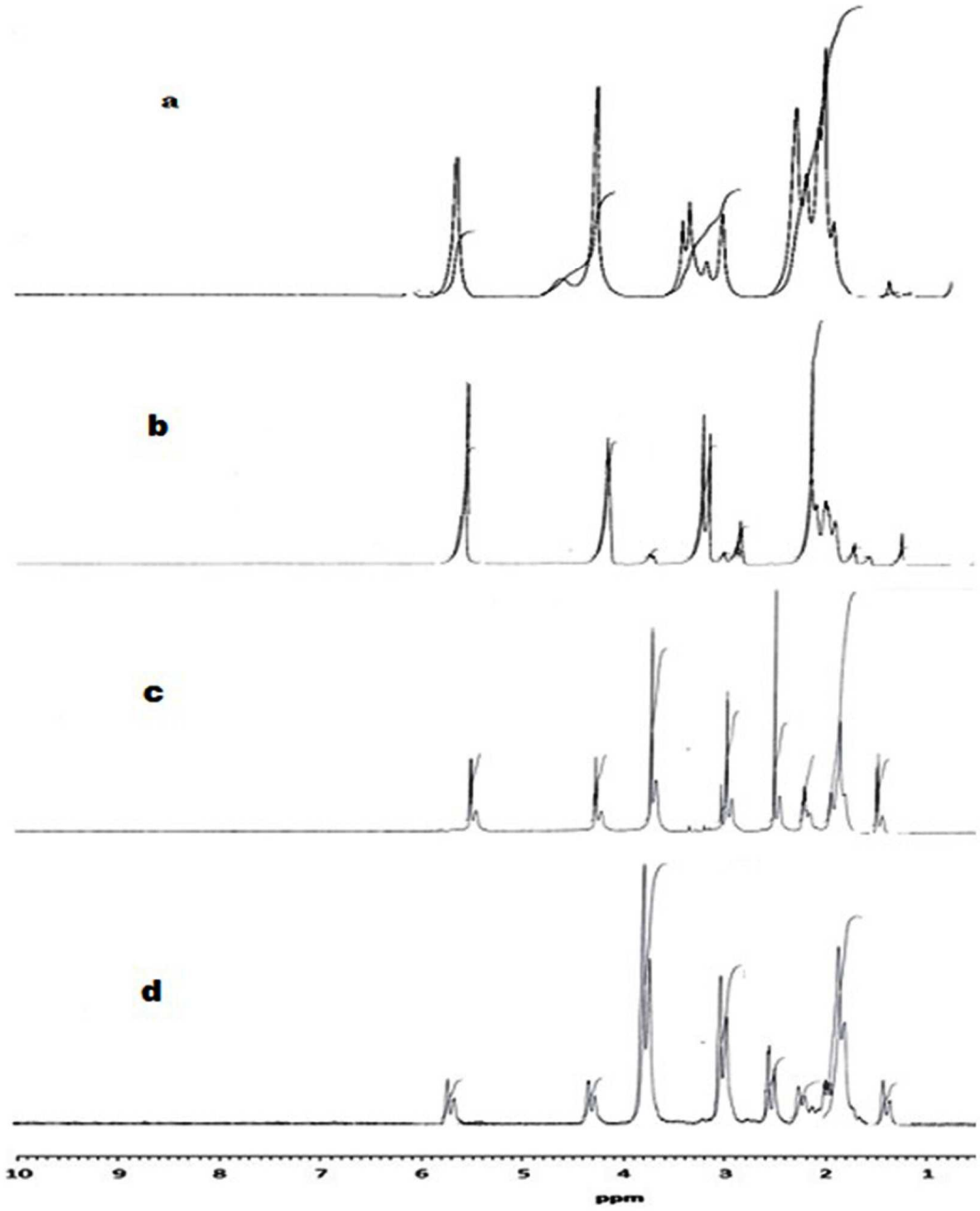

Fig. 3. ^{1}HNMR spectra of the synthesized alginate derived cationic surfactant and its metal complexes; (a) AS, (b) AS-Co, (c) AS-Cu and (d) AS-Zn

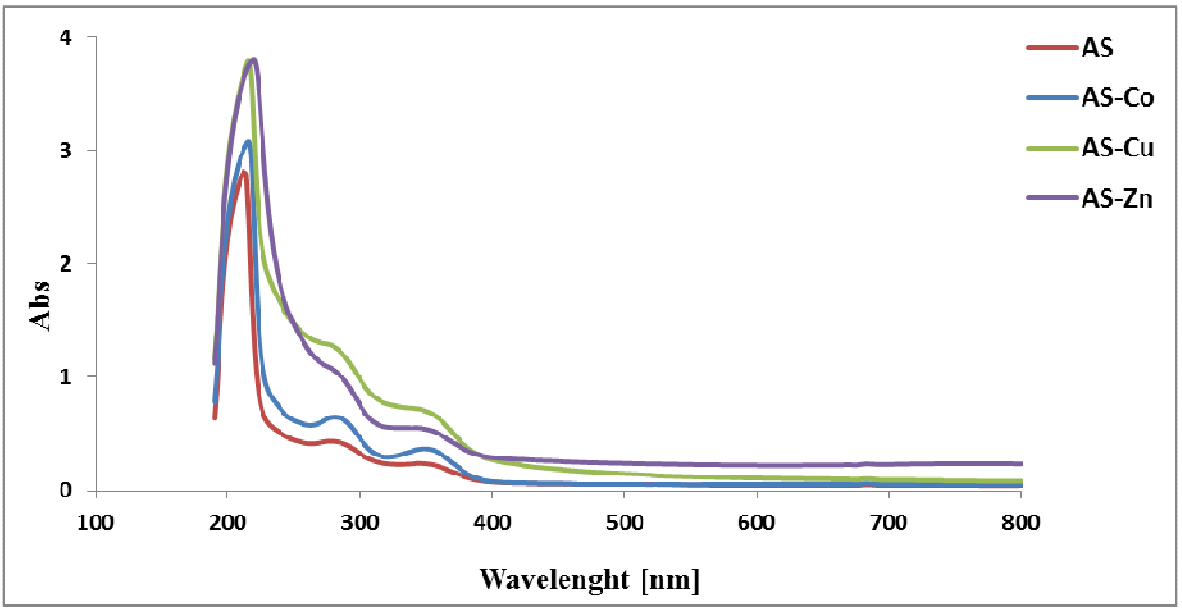

Fig. 4. UV-visible of the synthesized alginate derived cationic surfactant and its metal complexes

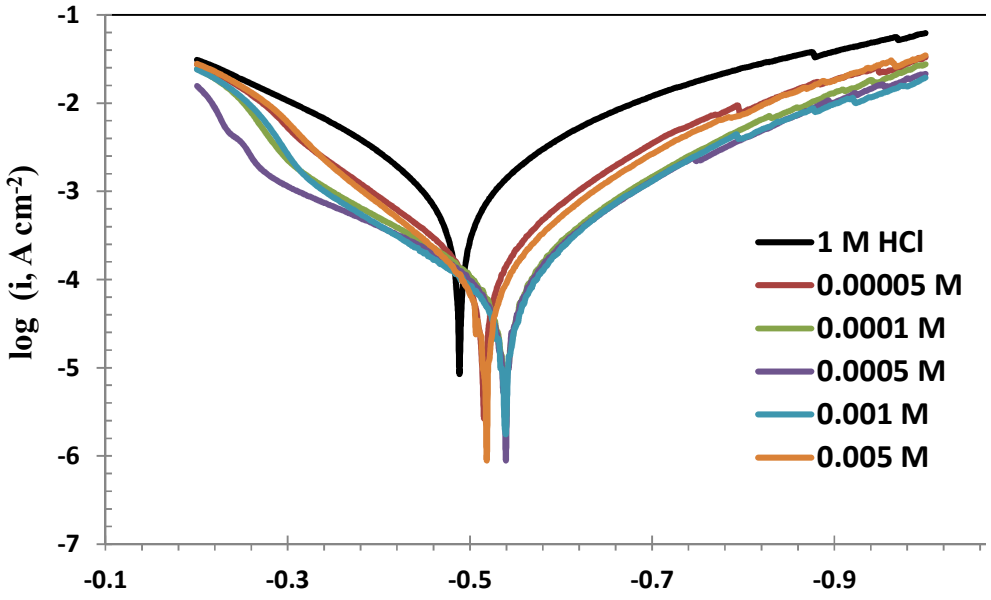

Fig. 5. Polarization curves for carbon steel in 1 M HCl in the absence and presence of different concentrations of inhibitor (AS) at 25 ^{o}C.

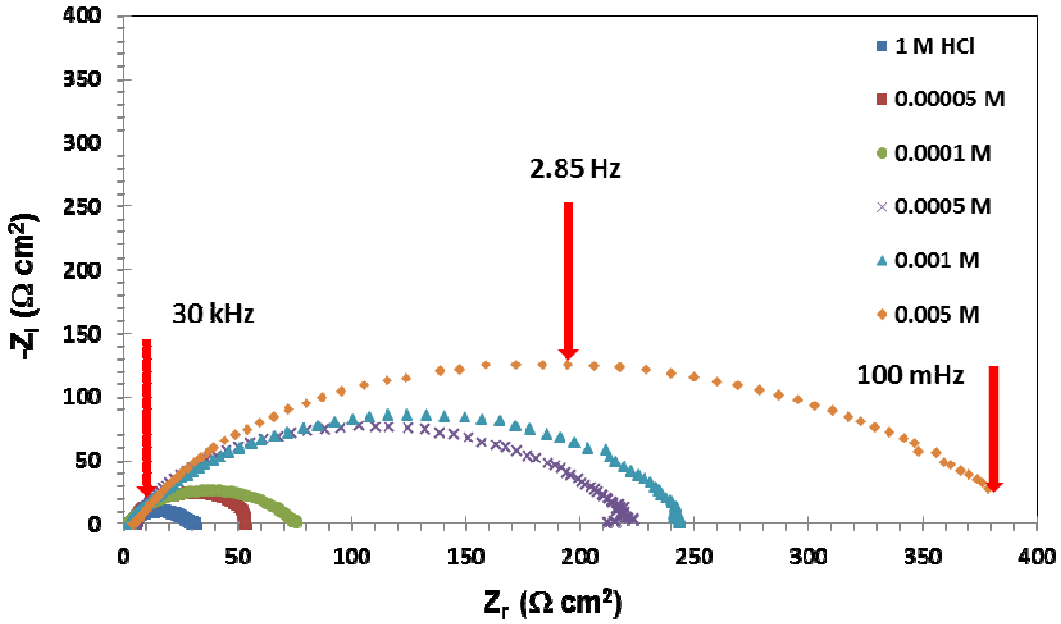

Fig. 6. Nyquist plots for CS in 1 M HCl in absence and presence of different concentrations of inhibitor (AS) at 25 ^{o}C

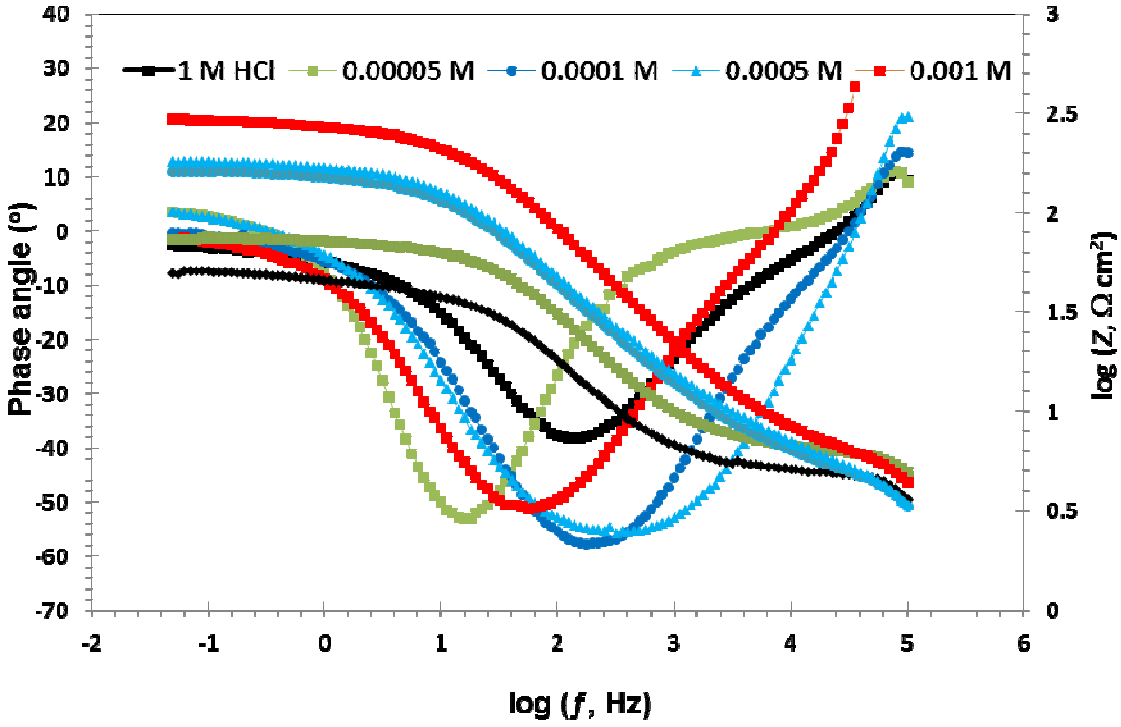

Fig. 7. Bode plots and phase angle for carbon steel in 1.0 M HCl in the absence and presence of different concentrations of the inhibitor (AS-Cu) **at 25 °C.**

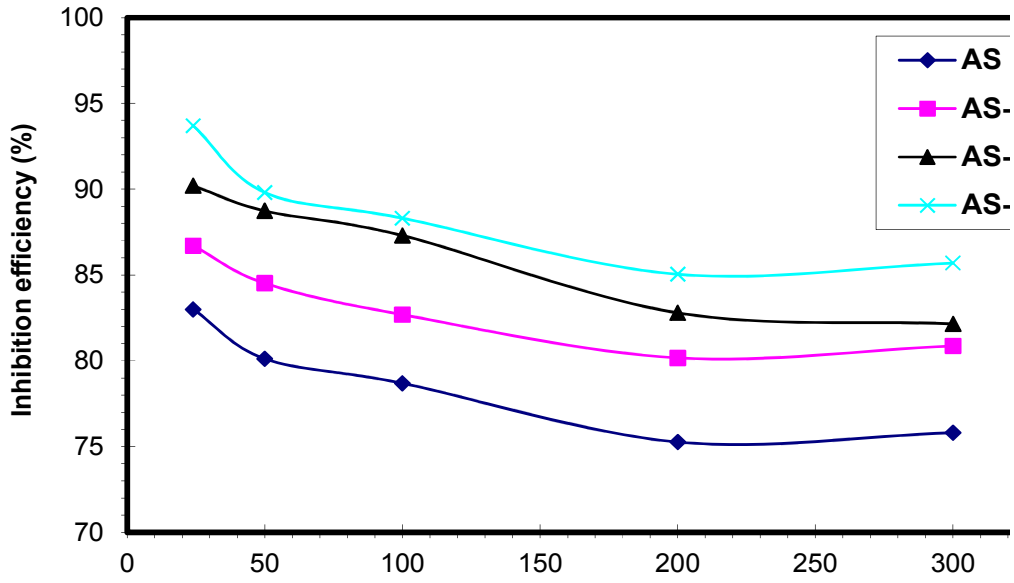

Fig.8. Variation of the inhibition efficiency of the synthesized inhibitors (AS, AS-Zn, AS-Co and AS-Cu) as a function of time at 25 °C .

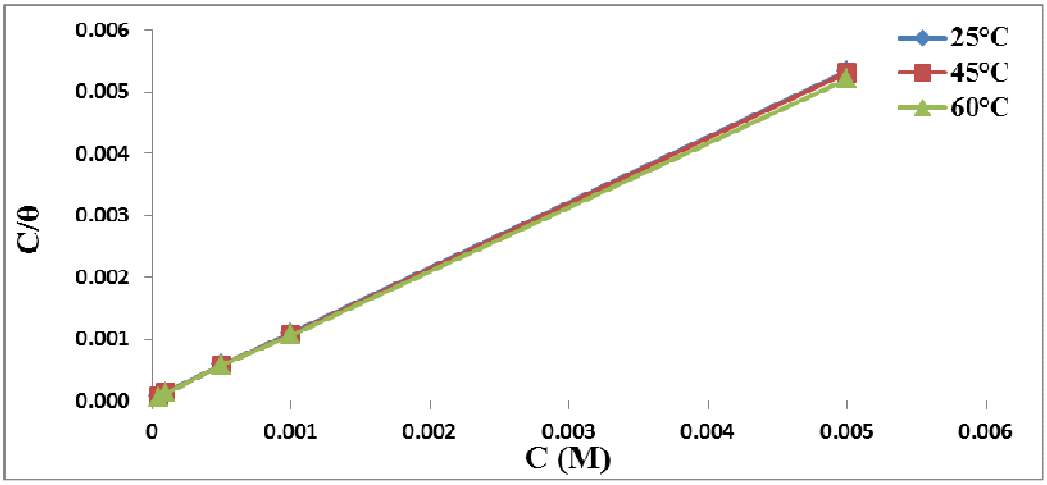

Fig. 9. Langmuir isotherm adsorption model of inhibitor (AS-Cu) on the carbon steel surface in 1 M HCl at different temperatures.

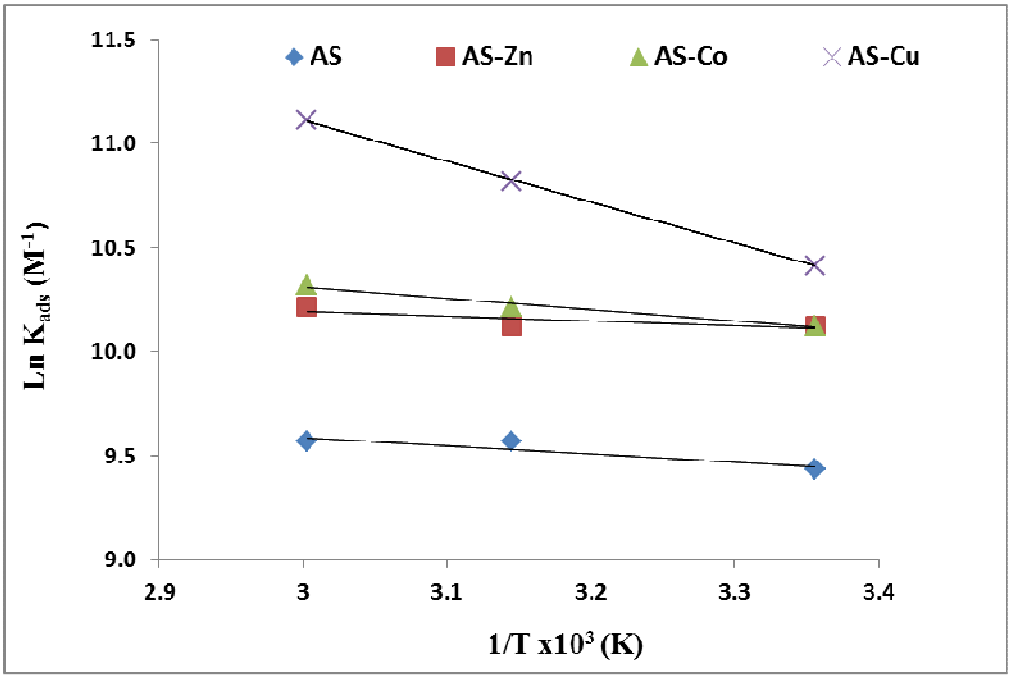

Fig. 10. The relationship between ln K_{ads} and 1/T for carbon steel in 1 M HCl solution containing different concentrations of inhibitors.

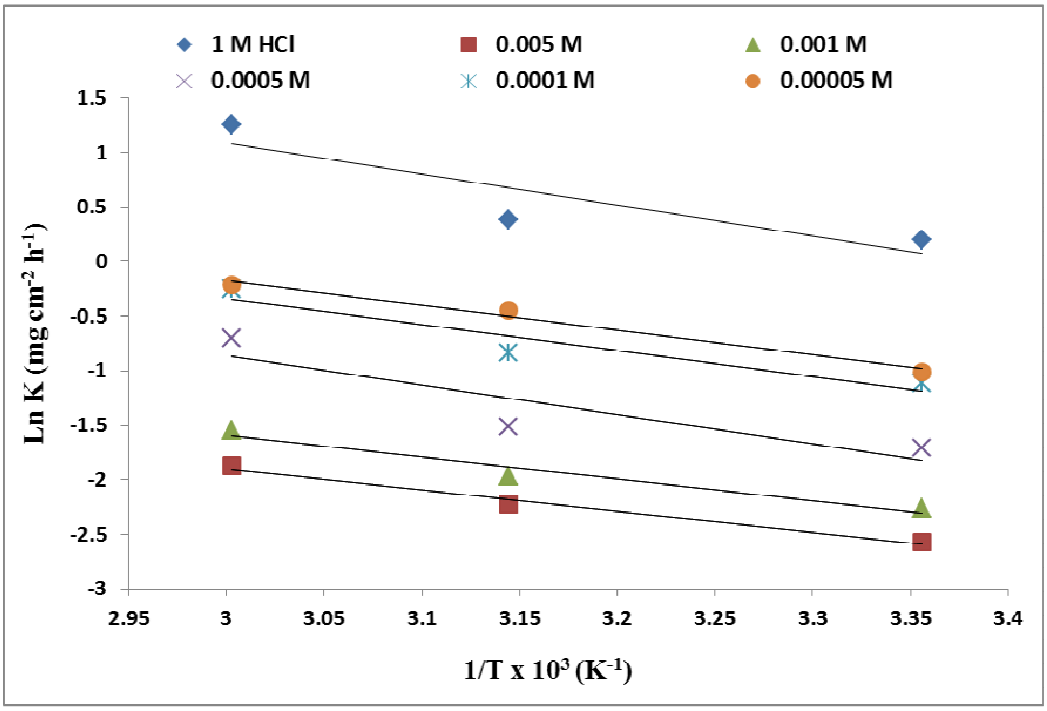

Fig. 11. ln k versus 1/T curves for carbon steel dissolution in absence and presence of different concentrations of inhibitor (AS-Cu) in 1 M HCl solution.

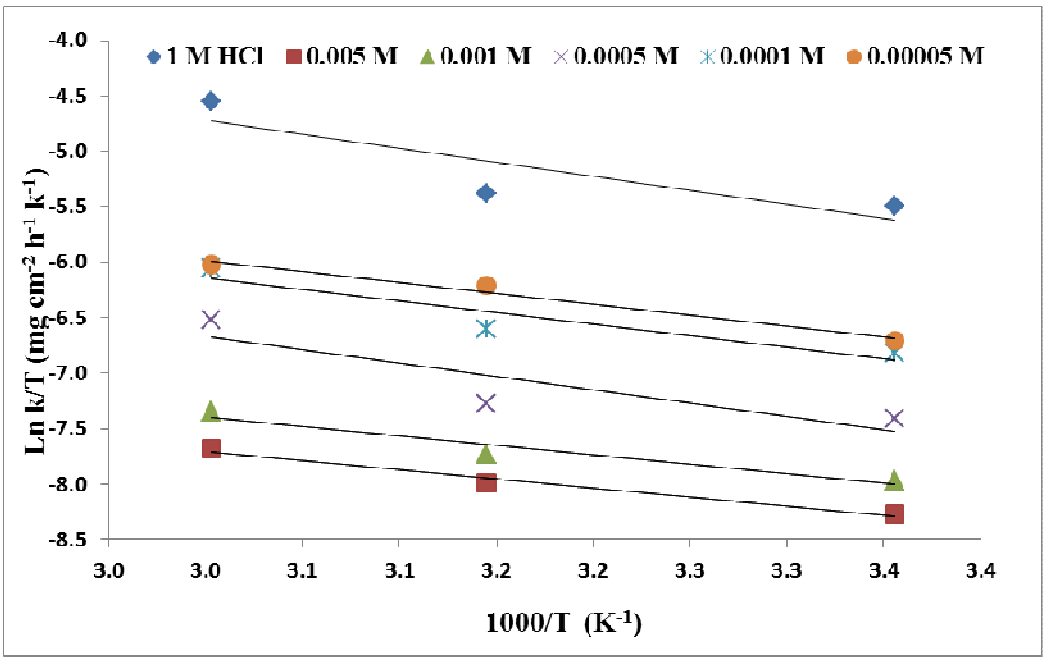

Fig. 12. Arrhenius plots of ln (k/T) versus 1/T for carbon steel in 1 M HCl solution without and with different concentrations of the synthesized inhibitor (AS-Cu)

Table 1. Potentiodynamic polarization parameters for corrosion of carbon steel in 1 M HCl in absence and presence of different concentrations of the synthesized inhibitors at 25 ^{o}C.

Inhibitor	Conc. of inhibitor (M)	- $E_{corr.}$ (mV(SCE))	$i_{corr.}$ ($mAcm^{-2}$)	β_a, ($mVdec^{-1}$)	- β_c, ($mVdec^{-1}$)	η_p %
Absence	0.00	491	0.735±0.0018	150	149	-----
AS	5 x 10^{-5}	517	0.235±0.0015	173	157	68.03
	1 x 10^{-4}	541	0.164±0.0011	246	168	77.69
	5 x 10^{-4}	541	0.144±0.0010	282	168	80.41
	1 x 10^{-3}	541	0.125±0.0080	226	158	82.99
	5 x 10^{-3}	520	0.088±0.0014	128	107	88.03
AS-Zn	5 x 10^{-5}	519	0.203±0.0017	160	167	72.38
	1 x 10^{-4}	518	0.155±0.0090	195	164	78.91
	5 x 10^{-4}	570	0.138±0.0010	348	169	81.22
	1 x 10^{-3}	562	0.118±0.0012	242	157	83.95
	5 x 10^{-3}	600	0.056±0.0015	399	121	92.38
AS-Co	5 x 10^{-5}	529	0.186±0.0021	190	166	74.69
	1 x 10^{-4}	542	0.141±0.0018	233	161	80.82
	5 x 10^{-4}	549	0.111±0.0012	234	155	84.90
	1 x 10^{-3}	577	0.094±0.0019	242	185	87.21
	5 x 10^{-3}	573	0.048±0.0011	223	129	93.47
AS-Cu	5 x 10^{-5}	533	0.170±0.0016	221	162	76.87
	1 x 10^{-4}	562	0.130±0.0015	280	167	82.31
	5 x 10^{-4}	509	0.076±0.0014	162	138	89.66
	1 x 10^{-3}	475	0.042±0.0013	115	213	94.29
	5 x 10^{-3}	484	0.033±0.0012	118	170	95.51

Table 2. EIS parameters for corrosion of carbon steel in 1 M HCl in absence and presence of different concentrations of the synthesized inhibitors at 25 ^{o}C.

Inhibitor	Conc. of inhibitor (M)	R_s,Ω cm^2	C_{dl},μF cm^{-2}	R_{ct}, Ω cm^2	η_I %
Absence	0.00	3.46	92.30	27.24±1.2	-----
AS	5×10^{-5}	5.19	656.3	48.49±1.2	43.82
	1×10^{-4}	3.12	554.4	71.76±1.0	62.04
	5×10^{-4}	4.53	36.39	215.2±1.1	87.34
	1×10^{-3}	3.92	41.79	240.6±0.9	88.68
	5×10^{-3}	3.78	185.7	383.8±19	92.90
AS-Zn	5×10^{-5}	3.37	67.43	66.08±1.7	58.78
	1×10^{-4}	4.51	60.30	166.7±1.5	83.66
	5×10^{-4}	5.16	54.08	185.9±2.4	85.35
	1×10^{-3}	4.52	136.4	368.5±2.3	92.61
	5×10^{-3}	1.96	96.27	462.8±1.4	94.11
AS-Co	5×10^{-5}	7.48	47.67	105.4±1.5	74.16
	1×10^{-4}	2.52	43.46	183±1.30	85.11
	5×10^{-4}	8.02	56.39	252.8±1.2	89.22
	1×10^{-3}	10.22	80.60	442.2±1.3	93.84
	5×10^{-3}	12.17	61.01	584.2±1.4	95.34
AS-Cu	5×10^{-5}	4.03	90.29	197.4±2.9	86.20
	1×10^{-4}	3.91	84.80	210.1±2.1	87.03
	5×10^{-4}	4.45	105.10	302.8±1.8	91.00
	1×10^{-3}	8.08	73.29	542.8±2.3	94.98
	5×10^{-3}	8.61	44.18	730.3±1.1	96.27

Table 3 .Weight loss data for carbon steel in 1 M HCl without and with different concentrations of the synthesized inhibitors at various temperatures.

Inhibitor	Conc. (M)	25 ^{O}C				45 ^{O}C				60 ^{O}C			
		ΔW mg	K (mg cm^{-2}h^{-1})	θ	η_w (%)	ΔW mg	k (mg cm^{-2}h^{-1})	θ	η_w (%)	ΔW mg	K (mg cm^{-2}h^{-})	θ	η_w (%)
Absence	0.00	1114± 1.11	1.220	-	-	1361.6±1.1	1.466	-	-	3559.2±1.3	3.923	-	-
AS	5 x 10^{-5}	479.9±0.63	0.529	0.56	56.4	50.9±0.77	0.426	0.60	60.4	999.9±1.11	1.102	0.72	71.9
	1 x 10^{-4}	388.6±0.44	0.428	0.65	64.7	42.2±0.22	0.047	0.67	67.2	961.7±0.91	1.060	0.73	73.0
	5 x 10^{-4}	307.9±0.41	0.339	0.72	72.0	34.2±1.10	0.038	0.73	73.4	883.0±0.45	0.973	0.75	75.2
	1 x 10^{-3}	300.3±0.60	0.331	0.73	72.7	28.1±0.55	0.031	0.78	78.1	681.6±0.66	0.751	0.81	80.8
	5 x 10^{-3}	187.3± 0.44	0.206	0.83	83.0	16.7±0.33	0.018	0.87	87.0	368.0±0.67	0.406	0.90	89.7
AS-Zn	5 x 10^{-5}	407.5±0.33	0.449	0.63	63.0	43.0±1.30	0.047	0.67	66.6	993.0±0.91	1.095	0.72	72.1
	1 x 10^{-4}	321.5±0.25	0.354	0.71	70.8	34.6±1.45	0.038	0.73	73.1	798.6±1.11	0.880	0.78	77.6
	5 x 10^{-4}	234.2±1.23	0.258	0.79	78.7	24.0±0.65	0.026	0.81	81.3	556.0±1.21	0.613	0.84	84.4
	1 x 10^{-3}	182.6±0.70	0.201	0.83	83.4	20.2±0.66	0.022	0.84	84.3	452.2±0.50	0.498	0.87	87.3
	5 x 10^{-3}	146.4±0.67	0.161	0.87	86.7	14.7±0.22	0.016	0.89	88.6	319.7±0.71	0.352	0.91	91.0
AS-Co	5 x 10^{-5}	370.6±0.80	0.409	0.66	66.3	40.6±0.31	0.045	0.68	68.4	920.6±1.66	1.015	0.74	74.1
	1 x 10^{-4}	311.2±0.82	0.343	0.72	71.7	29.2±1.60	0.032	0.77	77.3	799.2±0.22	0.881	0.78	77.5
	5 x 10^{-4}	191.8±0.55	0.211	0.83	82.6	19.8±1.71	0.022	0.85	84.6	431.8±0.21	0.476	0.88	87.9
	1 x 10^{-3}	141.7±1.45	0.156	0.87	87.1	14.7±1.44	0.016	0.89	88.6	381.7±0.55	0.421	0.89	89.3
	5 x 10^{-3}	107.5±1.55	0.118	0.90	90.2	11.5±1.55	0.013	0.91	91.1	301.5±1.81	0.332	0.92	91.5
AS-Cu	5 x 10^{-5}	331.0±1.10	0.365	0.70	69.9	35.8±1.66	0.039	0.72	72.2	731.0±0.91	0.806	0.79	79.5
	1 x 10^{-4}	296.3±0.90	0.327	0.73	73.1	28.3±1.10	0.031	0.78	78.0	708.3±0.33	0.781	0.80	80.1
	5 x 10^{-4}	163.4±0.55	0.180	0.85	85.1	17.4±0.37	0.019	0.86	86.5	447.4±0.21	0.493	0.87	87.4
	1 x 10^{-3}	94.0±0.61	0.104	0.91	91.5	9.0±0.91	0.010	0.93	93.0	194.0±0.55	0.214	0.95	94.5
	5 x 10^{-3}	69.5±0.88	0.077	0.94	93.7	7.5±0.41	0.008	0.94	94.2	139.5±0.88	0.154	0.96	96.1

Table 4: Thermodynamic parameters of adsorption on carbon steel surface in 1M HCl containing different concentrations of the synthesized inhibitors.

Inhibitor	T (^oC)	Slope	R^2	K_{ads} (M^{-1})x10^3	ΔG^0_{ads} (kJ mol^{-1})	ΔH^0ads (kJ mol^{-1})	ΔS^0ads (J $mol^{-1}K^{-1}$)
AS	25	1.131	0.9994	12.50	-33.3	3.3	111.7
	45	1.074	0.9995	14.29	-35.9		112.9
	60	1.001	0.9995	14.29	-37.6		112.9
AS-Zn	25	1.044	0.9999	25	-35.0	1.9	117.5
	45	1.082	0.9999	25	-37.4		117.5
	60	1.133	0.9999	33.33	-39.9		119.9
AS-Co	25	1.001	1	25	-35.0	5. 1	117.5
	45	1.020	1	33.33	-38.1		119.9
	60	1.098	1	50	-41.0		123.3
AS-Cu	25	1.160	1	33.33	-35.7	3.3	119.9
	45	1.050	1	50	-39.2		123.3
	60	1.080	0.9999	100	-43.0		129.0

Table 5: Activation parameters values for carbon steel in 1 M HCl in the absence and presence of different concentrations of the synthesized inhibitors

Inhibitor	Conc. of inhibitor (M)	E_a (kJ mol^{-1})	ΔH^*_{ads} (kJ mol^{-1})	ΔS^*_{ads} (J $mol^{-1}K^{-1}$)
AS	0.00	23.58	13.40	-173.73
	5×10^{-5}	17.38	14.40	-177.51
	1×10^{-4}	21.53	16.40	-187.31
	5×10^{-4}	24.22	19.17	-200.85
	1×10^{-3}	18.58	19.17	-213.00
	5×10^{-3}	16.10	26.27	-234.28
AS-Zn	5×10^{-5}	20.89	16.42	-189.79
	1×10^{-4}	21.54	18.31	-190.17
	5×10^{-4}	20.94	18.36	-192.80
	1×10^{-3}	21.94	18.96	-194.11
	5×10^{-3}	19.01	19.37	-204.50
AS-Co	5×10^{-5}	21.97	16.42	-186.87
	1×10^{-4}	22.34	18.31	-187.38
	5×10^{-4}	18.90	18.36	-189.33
	1×10^{-3}	23.66	18.96	-190.23
	5×10^{-3}	24.17	19.37	-203.21
AS-Cu	5×10^{-5}	18.94	13.59	-193.30
	1×10^{-4}	19.80	14.06	-197.07
	5×10^{-4}	22.50	16.33	-198.30
	1×10^{-3}	16.67	17.19	-216.86
	5×10^{-3}	16.21	19.89	-220.80